Anisotropic flow of charged and identified hadrons in the quark-gluon string model for Au+Au collisions at $\sqrt{s_{NN}} = 200$ GeV

G. Burau,[1] J. Bleibel,[1] C. Fuchs,[1] Amand Faessler,[1] L. V. Bravina,[2,3] and E. E. Zabrodin[2,3]
[1]*Institute for Theoretical Physics, University of Tübingen, Auf der Morgenstelle 14, D-72076 Tübingen, Germany*
[2]*Department of Physics, University of Oslo, Blindern 1048, N-0316 Oslo, Norway*
[3]*Skobeltzyn Institute for Nuclear Physics, Moscow State University, Vorobievy Gory, RU-119899 Moscow, Russia*
(Received 26 November 2004; published 31 May 2005)

The pseudorapidity behavior of the azimuthal anisotropy parameters v_1 and v_2 of inclusive charged ($h^{\pm}$) hadrons and their dependence on centrality has been studied in Au+Au collisions at full relativistic-heavy-ion-collider energy of $\sqrt{s_{NN}} = 200$ GeV within the microscopic quark-gluon string model (QGSM). The QGSM simulation results for the directed flow v_1 show antiflow alignment within the pseudorapidity range $|\eta| \leqslant 2$ in fair agreement with the experimental $v_1(\eta)$ data, but it cannot reproduce the further development of the antiflow up to $|\eta| \approx 3.5$. The η dependence of the elliptic flow v_2 extracted from the simulations agrees well with the experimental data in the whole pseudorapidity range for different centrality classes. The centrality dependence of the integrated elliptic flow of charged hadrons in the QGSM almost coincides with the PHOBOS experimental distribution. The transverse momentum dependence of the elliptic flow of identified ($\pi^{\pm}, K^{\pm}, p, \bar{p}$) and inclusive charged hadrons is studied also. The model reproduces quantitatively the low-p_T part of the distributions rather well, but it underestimates the measured elliptic flow for transverse momenta $p_T > 1$ GeV/c. Qualitatively, however, the model can reproduce the saturation of the $v_2(p_T)$ spectra with rising p_T as well as the crossing of the elliptic flow for mesons and baryons.

DOI: 10.1103/PhysRevC.71.054905 PACS number(s): 25.75.Ld, 24.10.Lx, 12.40.Nn

I. INTRODUCTION

Ultrarelativistic heavy-ion collisions (URHICs) offer an unique opportunity to study the nuclear phase diagram at high temperatures and densities [1]. The matter under such extreme conditions has probably existed in the early universe within the first few fm/c's after the big bang. Therefore, it is very tempting to investigate the properties of the little big bang [2] in the laboratory, and to search for a new state of matter, predicted by the fundamental theory of strong interactions (quantum chromodynamics, QCD), namely, a plasma of deconfined quarks and gluons (QGP).

Among the various experimental studies of URHICs operates the relativistic heavy-ion collider (RHIC) at BNL since 2000 to investigate gold-on-gold collisions up to $\sqrt{s_{NN}} =$ 200 GeV. After four years of operation, strong experimental evidence has been accumulated that at RHIC energies a new state of matter is indeed created which is qualitatively different from a hadron gas (see [1] and references therein). This state seems, however, not to behave like a weakly interacting parton gas—as could have been naively expected—but rather like a strongly coupled plasma. One argument toward such a scenario is the large elliptic flow observed at RHIC [3–6]. The development of strong elliptic flow requires short equilibration times and large pressure gradients to drive the dynamics, both being characteristic features of a strongly interacting system.

An independent argument for such a scenario is provided by lattice QCD, though still on a qualitative basis. While lattice QCD predicts undoubtedly a QGP phase transition around a critical temperature of $T_c \sim 150-180$ MeV, the properties of such a state are not yet so well understood. As a striking fact, lattice calculations do not reach the Stefan-Boltzmann limit for the pressure of a free parton gas $p \propto T^4$ even at $T \geqslant 5T_c$ but saturate around 80% of the Stefan-Boltzmann limit [7]. Taking this fact seriously and not as a lattice artefact, one may argue that the QGP at temperatures well above the critical one is still a strongly interacting system [8].

In line with these arguments goes the success of hydrodynamics in describing the collective flow at RHIC. Only at incident energies of $\sqrt{s_{NN}} \geqslant 130$ GeV (which corresponds to an initial energy deposit of about 10 GeV/fm^3 in the central reaction zone) does the hydrodynamic limit for the elliptic flow seem to be reached [9]. Within the limits of tuning the equation of state (including incorporation of a QGP phase transition), hydrodynamic calculations are able to rather reasonably describe the bulk properties of the collective flow [10–12]. However, when turning to more differential observables such as centrality dependence, mass dependence, or p_T dependence of the elliptic flow, hydrodynamic calculations also have some problems in matching the data.

In this context, it is also important to obtain an understanding of the reaction dynamics in terms of microscopic models. Microscopic models that have been very successfully applied at CERN super proton synchroton (SPS) energies and below are string models. The main assumption of string models is that hadrons are produced as a result of excitation and decay of open strings with different quarks or diquarks at their ends. Generally, all models are formulated as Monte Carlo event generators, allowing researchers to perform a careful analysis of the measurable quantities by introducing all necessary experimental cuts. There are numerous versions of the two basic string-motivated phenomenological approaches: the FRITIOF model [13] and the dual parton model (DPM) [14]. These two approaches use different mechanisms of string excitation. In

the first approach, which relies on relativistic classical string dynamics, the string masses arise from momentum transfer. The second one is based on the Gribov-Regge theory (GRT) [15] in the framework of relativistic quantum theory where quantum aspects like unitarity play an essential role. Here, the strings are produced as a result of color exchange.

By construction, such types of models do not contain explicitly a quark-hadron phase transition. However, during the temporal evolution of a heavy-ion reaction, a dense and strongly interacting plasma is formed within such approaches as well. The system consists of partons and color-flux tubes (or strings). Thus, an essential question is whether string models can create a sufficient amount of pressure in order to produce the large elliptic flow seen at RHIC, which features they can describe, and where they might fail. Such investigations are particularly relevant since transverse as well as elliptic flow at SPS energies is well reproduced within the string cascade approach [16–19]. By means of such studies, one can obtain deeper insight in to the question of which observables indicate the appearance of *new* physics not included in standard approaches to relativistic heavy-ion collisions.

In the present work, we describe ultrarelativistic heavy-ion reactions by a microscopic quark-gluon string model (QGSM) based on the Gribov-Regge theory. Details of the model are given in the next section. The QGSM has been demonstrated [20] to give a fair description of the first data of v_2 in Au+Au reactions at $\sqrt{s_{NN}} = 130$ GeV [3]. Here, we extend the analysis to full RHIC energy ($\sqrt{s_{NN}} = 200$ GeV) and to more differential observables, i.e., centrality dependence, mass dependence, and p_T dependence of v_1 and v_2.

II. QUARK-GLUON STRING MODEL

The quark-gluon string model (QGSM) incorporates partonic and hadronic degrees of freedom and is based on GRT accomplished by a string phenomenology of particle production in inelastic hadron-hadron (hh) collisions. To describe hadron-hadron, hadron-nucleus, and nucleus-nucleus collisions, the cascade procedure of multiple secondary interactions of hadrons was implemented. The QGSM incorporates string fragmentation, formation of resonances, and rescattering of hadrons, but simplifies the nuclear effects neglecting, e.g., the mean fields or evaporation from spectators. The QGSM includes as independent degrees of freedom octet and decuplet baryons, octet and nonet vector and pseudoscalar mesons, and their antiparticles. The momenta and positions of nucleons inside the nuclei are generated in accordance with the Fermi momentum distribution and the Woods-Saxon density distribution, respectively. Pauli blocking of occupied final states is taken into account. Strings in the QGSM can be produced as a result of the color exchange mechanism or, as in diffractive scattering, they can be due to momentum transfer. The Pomeron, which is a pole with an intercept $\alpha_P(0) > 1$ in the GRT, corresponds to the cylinder-type diagrams. The s-channel discontinuities of the diagrams, representing the exchange by n Pomerons, are related to the process of $2k(k \leqslant n)$ string production. If the contributions of all n-Pomeron exchanges to the forward elastic scattering amplitude are known, the Abramovskii-Gribov-Kancheli (AGK) cutting rules [21] enable one to determine the cross sections for $2k$ strings. Hard gluon-gluon scattering and semihard processes with quark and gluon interactions are also incorporated in the model [22]. The inclusive spectra in the QGSM have automatically the correct triple-Regge limit for the Feynman variable $x \to 1$and the double-Regge limit for $x \to 0$, and they satisfy all conservation laws [23]. The particular stages of the collision model, namely (i) initialization of interacting projectile and target nuclei, (ii) string formation via inelastic nucleon-nucleon (hadron-hadron) interaction, (iii) string fragmentation, i.e., hadronization, and (iv) hadron-hadron rescattering, are solved basically by Monte Carlo simulation techniques [24].

III. ANISOTROPIC FLOW OF INCLUSIVE CHARGED AND IDENTIFIED HADRONS

Among the main signals that can help reveal the formation of the QGP in the experiment are collective flow phenomena. Flow is directly linked to the equation of state (EOS) of the excited matter. Generally, an effective EOS extracted from model studies shows "softness" during the early stages of the collision, but it remains unclear whether the observed softness is due to (i) the proximity of the QCD phase transition [25–28], (ii) nonequilibrium phenomena, such as the formation and fragmentation of strings [29,30], or (iii) nuclear shadowing [16,17,31].

The transverse collective flow can be subdivided into isotropic and anisotropic flow. Two types of anisotropic flow, which are characterized by the first and the second harmonic coefficients of the Fourier decomposed invariant azimuthal distribution in momentum space [32,33]

$$E\frac{d^3N}{d^3p} = \frac{1}{\pi}\frac{d^2N}{dp_T^2 dy}\left[1 + 2\sum_{n=1}^{\infty} v_n(p_T, y)\cos(n\phi)\right], \quad (1)$$

are called *directed* and *elliptic* flow. Here, $p_T = (p_x^2 + p_y^2)^{1/2}$ is the transverse momentum, y the rapidity, and ϕ the azimuthal angle between the particle's momentum and the reaction plane. While the elliptic flow $v_2 = \langle\cos(2\phi)\rangle = \langle(p_x/p_T)^2 - (p_y/p_T)^2\rangle$ is assumed to be particularly sensitive to pressure at the early stages of the collisions [10,20,30,34], the directed flow appears to develop until the late stage of the heavy-ion reaction [16–18]. On the other hand, the directed flow of particles with high transverse momentum, which are emitted at the onset of the collective expansion, can carry information about the EOS of the dense matter phase from the initial conditions. A lot of measurements of the v_2 parameter in Au+Au collisions at RHIC have been performed for charged and identified hadrons, see [3–6] and references therein, whereas experimental results for the directed flow v_1 at RHIC has been reported only quite recently [35,36].

A. Directed flow of inclusive charged hadrons

Figure 1 depicts the QGSM simulation result for the pseudorapidity dependence of the directed flow $v_1(\eta)$ of

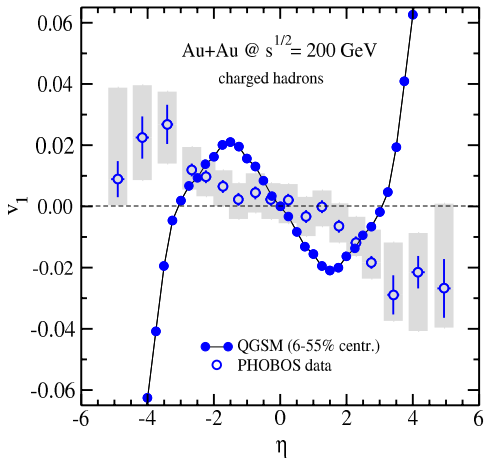

FIG. 1. (Color online) Directed flow v_1 for charged hadrons as a function of pseudorapidity η in comparison to the result from the PHOBOS Collaboration (centrality 6 to 55%) [36] for Au+Au collisions at $\sqrt{s_{NN}} = 200\,\text{GeV}$. Statistical (bars) and systematic (boxes) experimental errors are shown.

charged hadrons compared to the experimental data from the PHOBOS Collaboration [36] for 6 to 55% central Au+Au collisions at $\sqrt{s_{NN}} = 200\,\text{GeV}$. (QGSM predictions for the directed flow of identified particles at lower RHIC energy, $\sqrt{s_{NN}} = 130\,\text{GeV}$, can be found in [37].) One can see that the model reproduces the v_1 data quite well both qualitatively and quantitatively, although the maxima of the directed flow around $|\eta| \approx 2$ are shifted to lower pseudorapidities compared to the experimental data. The $v_1(\eta)$ result shows a characteristic wiggle structure with a clear antiflow[1] component in the middle $|\eta|$ region. It was pointed out in [38] (see also [17,39]) that the phenomenon leading to the formation of a wiggle structure for the directed flow of nucleons is caused by dense baryon-rich matter shadowing, which plays a decisive role in the competition between normal flow and antiflow in noncentral nuclear collisions at ultra relativistic energies. Within microscopic string model calculations, such deviations from the straight line behavior of the nucleonic flow were first observed in very peripheral Au+Au collisions at AGS energy [31]. Experimentally, the wiggle structure of v_1 for protons in peripheral Pb + Pb collisions at SPS has been observed by the NA49 Collaboration [40,41]. However, the QGSM distributions of $v_1(\eta)$ at these lower energies also have peaks which are shifted by approximately one unit of rapidity toward $\eta = 0$ [16,17,29] compared to the experimental data. So, this shift, which also leads to a steeper slope in the midrapidity region, seems to be a sort of model "artefact" occurring at higher collision energies as well. The question about the origin of the directed flow's rapidity dependence obtained within the QGSM is not so easily answered. One reason might be the lack of heavy resonances in the model compared, e.g., to the ultrarelativistic quantum molecular dynamics (UrQMD) model [42] or the multiphase transport (AMPT) model [43]. These resonances are mostly concentrated in the rapidity regions of flying away spectators which exhibit normal flow. Lighter particles coming from the decays of the heavy resonances, each moving in the normal direction and having nearly the same rapidity, may significantly enhance the normal component of the directed flow in a pseudorapidity range closer to the fragmentation region. The total multiplicity of particles with pseudorapidity $|\eta| > 3.5$ is quite low in the present version of the QGSM. The complex connection between the model dynamics of the QGSM and the characteristics of the resulting directed flow requires further lucid investigations to understand in detail the origin of the change in sign, and in particular the strong antiflow behavior of $v_1(\eta)$ in the midrapidity region.

Nevertheless, our picture is a bit different compared to that provided by the microscopic models based on the FRITIOF routine. For instance, the relativistic quantum molecular dynamics (RQMD) model favors weak but still normal flow for pions [38] even for more peripheral topologies with $b = 5-10\,\text{fm}$, corresponding to a centrality range $\sigma/\sigma_{\text{geo}} = 15-60\%$. Both the UrQMD model and the AMPT model show a very flat and essentially zero directed flow [42,43] in a broad range $|\eta| \leqslant 2.5$. It is worth mentioning here that the results of both models have been obtained for minimum bias, not semiperipheral, events. Although the data seem to indicate antiflow behavior for the directed flow of charged particles with the possible flatness at $|\eta| \leqslant 1.5$, the measured signal is quite weak, the magnitude of the flow is less than 1% at $|\eta| \leqslant 2$. Therefore, relatively large systematic error bars do not permit us to disentangle between the different models.

Similar antiflow alignment can be obtained also within the multimodule model (MMM) [44], which is based on fluid dynamics coupled to the formation of color ropes. In this model, the effect of the tilted initial state, responsible for the antiflow formation, reaches its maximum for the impact parameter $b \approx 0.5(R_A + R_B)$, i.e., for the centrality $\sigma/\sigma_{\text{geo}} \approx 25\%$ in case of a symmetric system of colliding nuclei. To check the centrality dependence of the directed flow at full RHIC energy, the pseudorapidity distributions $v_1(\eta)$ of nucleons and charged pions in Au+Au collisions at $\sqrt{s_{NN}} = 200\,\text{GeV}$ are displayed in Fig. 2 for six different impact parameters b going from central (upper left panel) to very peripheral (lower right panel) configurations. Regardless of the centrality range, the directed flow of pions has negative slope, i.e., antiflow, in the midrapidity range. For nucleons, the azimuthal anisotropy parameter v_1 is small for central collisions ($b = 2\,\text{fm}$). In accord with our previous studies and conclusions [16,17], for Au+Au collisions at full RHIC energy, deviations of nucleonic flow from a normal flow behavior occur already at quite small impact parameters. This means that the effect is indeed shifted to more central configurations. With the increase of b, these deviations, representing the wiggle structure of the flow, appear more distinctly. However, the QGSM simulations for both nucleonic and pionic flow at midrapidity $|\eta| \leqslant 1$ are consistent with the zero flow signal $v_1 = 0$. The other features which should be mentioned here are the broadening of the antiflow region and the increase of its strength as the reaction

[1]Conventionally, the type of flow with positive slope $dv_1/d\eta$ is called *normal flow*, in contrast to *antiflow* for which $dv_1/d\eta$ is negative.

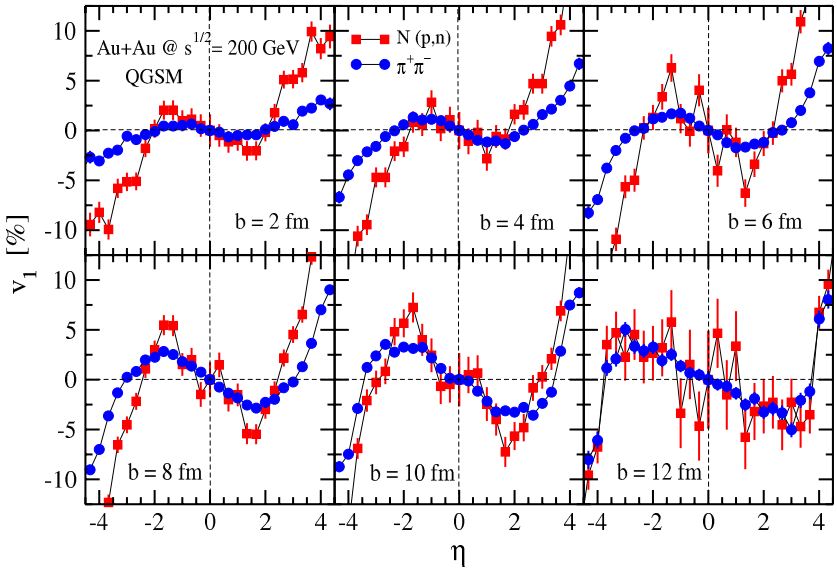

FIG. 2. (Color online) Directed flow v_1 for nucleons and charged pions from $\sqrt{s_{NN}} = 200$ GeV Au+Au reactions as a function of pseudorapidity η for six different impact parameters b going from central ($b = 2$ fm) to peripheral ($b = 12$ fm) collisions. Only statistical errors are shown.

becomes more peripheral. Therefore, one can disentangle between two processes of different origin employed for the description of the *third-flow component*: If the formation of nucleonic antiflow is dominated by the creation of QGP, the flow maximum is reached at $b \leqslant 6$ fm [44], whereas for the shadowing scenario the strong antiflow should be observed also in very peripheral events with $b \approx 10$ fm.

B. Elliptic flow of charged and identified hadrons

Here we investigate the pseudorapidity dependence of the elliptic flow of charged hadrons. The QGSM simulation result for minimum bias Au+Au collisions at $\sqrt{s_{NN}} = 200$ GeV are compared in Fig. 3 with the experimental data of the PHOBOS Collaboration [5]. The elliptic flow displays a strong in-plane alignment in accordance with the predictions of Ref. [34]. At midrapidity $|\eta| < 1.0$, the elliptic flow is almost constant. Then it rises up slightly and drops rapidly at $|\eta| > 2.0$ with increasing pseudorapidity. The mean value of $v_2^{\rm ch}(|\eta| \leqslant 2.5)$ is practically as large as the value measured by the PHOBOS Collaboration at midrapidity. The experimental data, which indicate a steady decrease in v_2 with increasing $|\eta|$, are slightly overestimated by the model only at $|\eta| \approx 2.0$ as a consequence of a double hump structure in the theoretical result. This difference in shape close to $\eta = 0$ still rankles somewhat, although within the error bars the pseudorapidity dependence of the elliptic flow of charged hadrons obtained within the QGSM shows a really fair agreement with the PHOBOS data [5] in the whole η range.

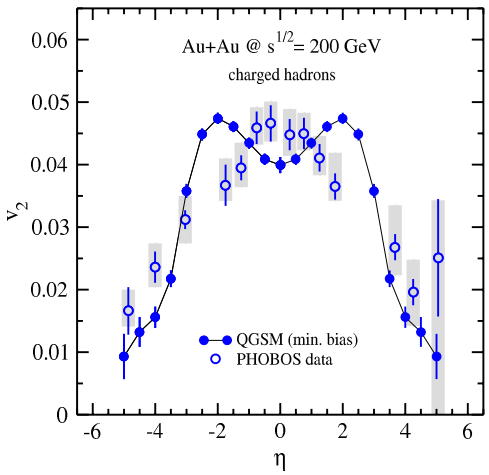

FIG. 3. (Color online) Elliptic flow v_2 for inclusive charged hadrons as a function of pseudorapidity η in comparison with the PHOBOS data of minimum bias Au+Au collisions at $\sqrt{s_{NN}} = 200$ GeV [5]. The systematic errors of the experimental data are shown as gray boxes together with the statistical errors (bars), respectively.

However, following the idea of longitudinal boost invariance[2] of the expanding hot and dense matter and the common interpretation of elliptic flow as a consequence of secondary particle collisions, one would expect no or at least a weak pseudorapidity dependence of v_2 similar to that of the multiplicity density $dN/d\eta$ over a large rapidity range. The experimentally observed multiplicity stays approximately constant within three units of pseudorapidity [45], while the elliptic flow data show a pronounced peak at midrapidity [5,46]. This is somehow in contradiction with the assumption of longitudinal boost invariance over a broad region of rapidity in RHIC collisions. Most of the hydrodynamics calculations reported in the literature are based on boost invariant models. Therefore, the results obtained within such approaches are independent of rapidity, and one is limited to discuss only the transverse behavior [47]. Hydrodynamics results for the pseudorapidity dependence of v_2 are scarce.

[2]The assumption of a longitudinal boost invariant system means that its energy density and pressure do not depend on the longitudinal coordinate z compared at the same proper time $\tau = \sqrt{t^2 - z^2}$. In other words, the evolution of the pressure and energy density depends only on τ but not on η.

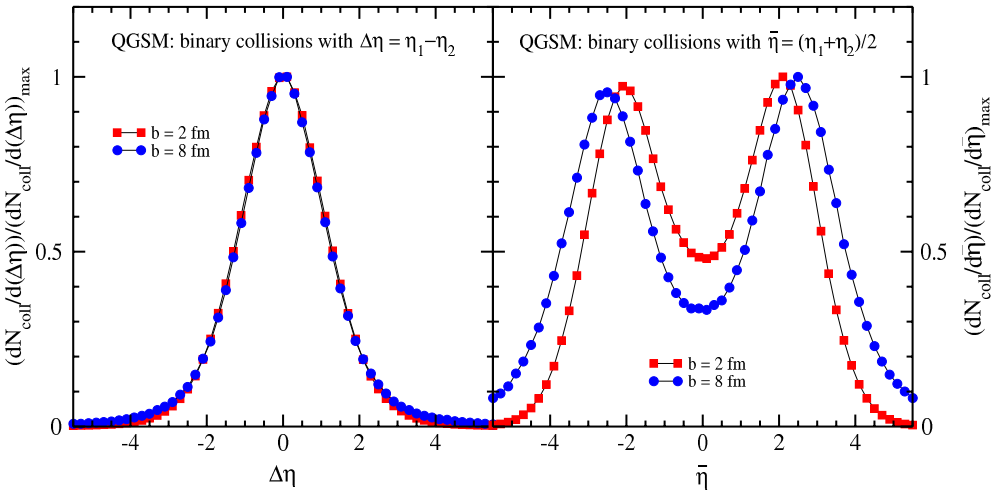

FIG. 4. (Color online) Number of binary particle collisions per pseudorapidity interval normalized to its maximum as function of the pseudorapidity difference $\Delta\eta = \eta_1 - \eta_2$ (left) and the mean pseudorapidity $\bar{\eta} = (\eta_1 + \eta_2)/2$ (right) of the two colliding particles. The QGSM results are obtained for simulated Au+Au reactions at $\sqrt{s_{NN}} = 200\,\text{GeV}$ with two different impact parameters b.

The shape of $v_2(\eta)$ in Au+Au collisions at $\sqrt{s_{NN}} = 130\,\text{GeV}$ studied within a full three-dimensional hydrodynamic model by Hirano *et al.* [48–50] shows a bump structure in forward and backward rapidity regions, when the initial energy density profile depends strongly on the space-time rapidity η_s. The bumps appear at the same rapidity regions where the initial configuration is no longer boost invariant. In the case of an almost η_s independent deformation of the initial energy density, the resultant $v_2(\eta)$ has no bumps. Thus it was shown in [50] that the pseudorapidity dependence of the elliptic flow is highly sensitive to the parametrization of the initial energy density profile in the longitudinal direction. The initial energy density profile in microscopic transport models is not explicitly parametrized, but it is implicitly fixed by the initial conditions of the projectile and target nucleus. The elliptic flow studied within the UrQMD model in the cascade mode shows also a prominent dip at central rapidities for all inspected hadrons [42]. There it is argued that this rapidity behavior of v_2 indicates a region of small interaction strength (or low "pressure") because of the direct connection between the strength of the anisotropic flow and the mean free path of the particles forming the hot midrapidity region. Therefore, the appearance of the dip in v_2 is linked to a feature of the model dynamics in the early stage, namely the preequilibrium string dynamics and interactions on the parton level [42]. Also in the QGSM, the emergence of the double bump structure in $v_2(\eta)$ is strongly connected with the model dynamics, as one can clearly see in the time evolution of the elliptic flow and its rapidity dependence [51]. The normalized number of binary particle collisions per pseudorapidity interval throughout the evolution of the system as a function of the pseudorapidity is depicted in Fig. 4 for two impact parameters $b = 2\,\text{fm}$ and $b = 8\,\text{fm}$ to show the strong correlation between the particle interactions and the flow strength mainly produced by secondary collisions. First of all, this number versus the pseudorapidity difference $\Delta\eta = \eta_1 - \eta_2$ of the two colliding particles is plotted in the left panel of Fig. 4. The peak around $\Delta\eta = 0$ indicates unambiguously that independently of the impact parameter, the particles with equal or at least very similar rapidities most likely interact. The plot on the right-hand side of Fig. 4, where the number of binary collisions normalized to its maximum is shown as a function of the mean pseudorapidity $\bar{\eta} = (\eta_1 + \eta_2)/2$ of the two colliding particles, is even more instructive. Here, a clear double peak structure appears in the same rapidity region as seen in Fig. 3 for the η dependence of the elliptic flow. The dip in the number of collisions around $\bar{\eta} = 0$ becomes more pronounced with decreasing centrality. In addition, the two peaks for $b = 8\,\text{fm}$ are slightly shifted to higher pseudorapidities compared with the result for $b = 2\,\text{fm}$. This is nicely consistent with the centrality dependence of $v_2(\eta)$ obtained within the QGSM, as will be discussed later.

Figure 5 presents the pseudorapidity distribution of the elliptic flow for charged hadrons in gold-gold collisions at full RHIC energy for three different centrality classes, ranging from central (bottom panel) via midcentral (middle panel) to peripheral (top panel) in accordance with the definitions in [5]. The results are overlaid from the QGSM simulation and the PHOBOS analysis (combined data from the hit- and track-based methods). The model is able to describe the magnitude and shape of $v_2^{\text{ch}}(\eta)$ quite well across all of the three centrality bins within the given systematic and statistical uncertainties. The overall shape of the η distribution changes only very little with centrality and shows a behavior very similar to that depicted in Fig. 3 for the minimum bias events. The two-peak structure of $v_2^{\text{ch}}(\eta)$ in the interval $|\eta| \leqslant 2.5$, which is clearly seen for simulated peripheral collisions but "washed out" in the central bin, is not attributed solely to QGSM, but arises also in, e.g., UrQMD calculations [42] as discussed in detail above. However, the effect is small, and the mean value of the v_2^{ch} parameter over the aforementioned range increases from central to peripheral collisions in good quantitative agreement with the experimental data. This is not a trivial result, because neither the pseudorapidity nor the

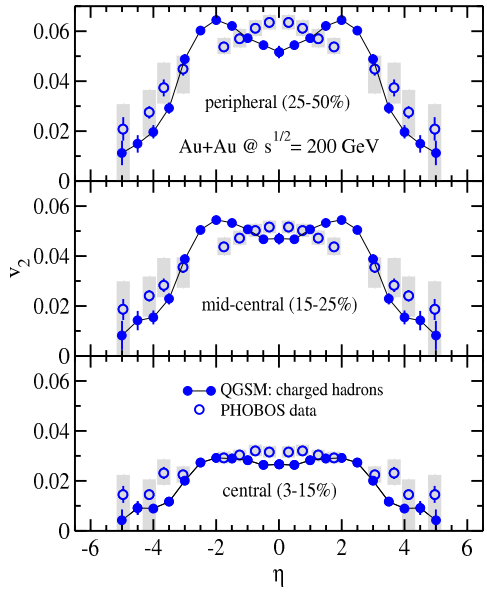

FIG. 5. (Color online) Elliptic flow v_2 for inclusive charged hadrons from $\sqrt{s_{NN}} = 200\,\text{GeV}$ Au+Au collisions as a function of pseudorapidity η for the three centrality classes according to the PHOBOS analysis (combined hit- and track-based results) [5]. Again, the systematic errors of the experimental data are shown as gray boxes together with the statistical error bars, respectively.

centrality dependence of the elliptic flow, which is discussed below, is reproduced correctly at RHIC so far by the UrQMD calculations and hydrodynamic models.

The next observable is the transverse momentum dependence of v_2 for identified hadrons, namely, combined $\pi^+ + \pi^-$, $K^+ + K^-$, as well as $p + \bar{p}$ spectra in minimum bias Au+Au collisions at $\sqrt{s_{NN}} = 200\,\text{GeV}$. The QGSM simulation results are depicted in Figs. 6 and 7 in comparison to the PHENIX [6] and STAR data [52], respectively.

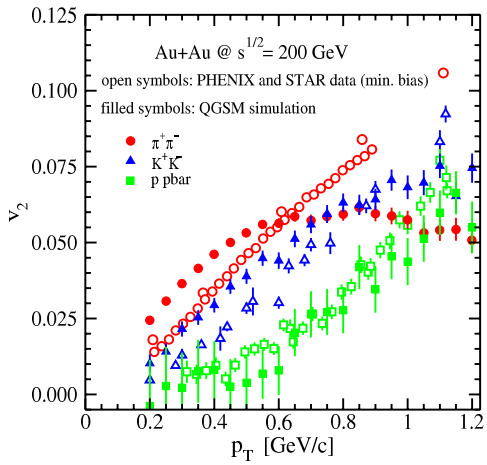

FIG. 6. (Color online) Transverse momentum dependence of v_2 for identified hadrons $\pi^+ + \pi^-$, $K^+ + K^-$, $p + \bar{p}$ in the low-p_T range $0.0 \leqslant p_T \leqslant 1.0\,\text{GeV}/c$ for minimum bias Au+Au collisions at $\sqrt{s_{NN}} = 200$ GeV. The experimental data are PHENIX [6] and STAR [52] results. Only statistical errors are shown.

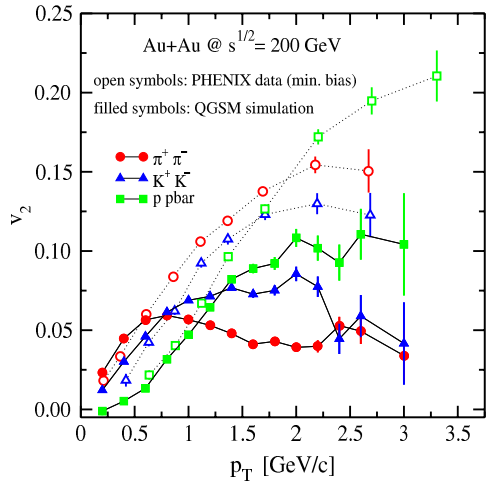

FIG. 7. (Color online) The same as in Fig. 6, but in the overall p_T range $0.0 \leqslant p_T \leqslant 3.5\,\text{GeV}/c$. The PHENIX data are taken from [6].

The agreement with the experimental data at least for protons/antiprotons and kaons is rather good in the range of low transverse momenta $0.0 \leqslant p_T \leqslant 1.0\,\text{GeV}/c$, as illustrated in Fig. 6. The steady increase of the elliptic flow with rising p_T and the larger v_2 parameter at a given p_T for the lighter mass hadrons compared to the heavier ones is well reproduced by the model calculation. For pions, the latter statement is only valid for the transverse momenta below $0.75\,\text{GeV}/c$. The elliptic flow of charged pions already starts to saturate at $p_T > 0.5\,\text{GeV}/c$. This early saturation of the pionic v_2 continues with a slight decrease at increasing p_T and entails the peculiar result to be smaller than the kaon flow for transverse momenta between 1.0 and $2.5\,\text{GeV}/c$, as shown for the overall p_T range in Fig. 7.

This deviation compared to the experimental findings is remarkable because it was shown in [20] that the magnitude of the pionic flow in the QGSM calculations is already twice as large as obtained, e.g., in the RQMD ones. It has been elaborated in [20] that the contributions of hard processes and multi-Pomeron exchanges are very important to reaching the reported magnitude of v_2 and correctly reproducing the particle multiplicities. To confirm the latter statement, the transverse mass spectra of positively and negatively charged pions and kaons for pp collisions at $\sqrt{s_{NN}} = 200\,\text{GeV}$ are presented in Fig. 8. The m_T spectra obtained within the full version of the QGSM, which incorporates hard and multichain contributions, are in good agreement with the experimental spectra reported by the STAR Collaboration [53].

Coming back to the p_T behavior of the elliptic flow depicted in Fig. 7, it is important to stress at this point another striking feature of the QGSM. Namely, this model is able to reproduce at least qualitatively the experimental evidence of the crossing of the elliptic flow for mesons and baryons at $p_T \approx 1.7\,\text{GeV}/c$ [6]. The simulation data show that at $p_T < 1.4\,\text{GeV}/c$, the v_2 parameter for kaons is larger than for (anti)protons. At higher transverse momenta $p_T > 1.4\,\text{GeV}/c$, the situation is completely changed. Here, the elliptic flow of protons and

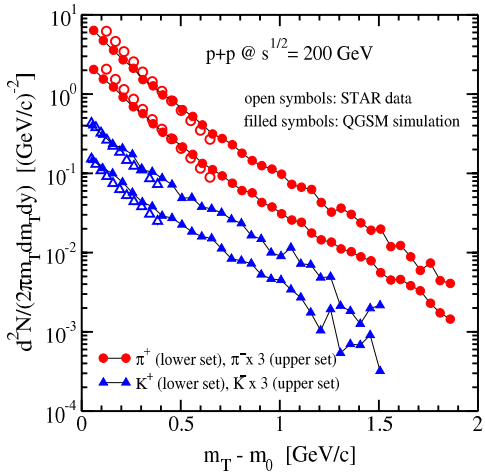

FIG. 8. (Color online) Transverse mass spectra of $\pi^{\pm}$ and $K^{\pm}$ for simulated pp collisions at $\sqrt{s_{NN}} = 200\,\mathrm{GeV}$ compared to the STAR data [53].

antiprotons becomes larger than v_2 for charged kaons and pions.

This behavior is also described within the quark recombination models [54–57], which assume the statistical coalescence of two or three quarks into a hadron. In contrast, the hydrodynamic picture shows the same mass ordering for the elliptic flow of different particles at all transverse momenta [11]. We will come to this point after the study of $v_2(p_T)$ for inclusive charged hadrons. The QGSM distributions are shown in Fig. 9 in comparison to the experimental data of the PHOBOS and PHENIX Collaborations [5,6]. To demonstrate the importance of rescattering processes for the elliptic flow formation, the v_2^{ch} extracted from a QGSM simulation run for minimum bias Au+Au collisions without the hadronic cascade is additionally plotted in this figure. It is quite obvious that the model without subsequent secondary interactions

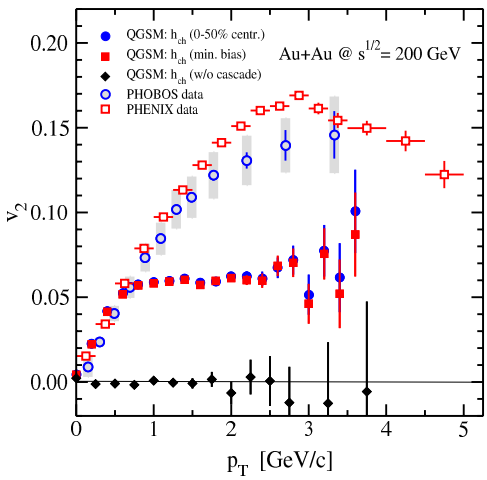

FIG. 9. (Color online) Elliptic flow v_2 for inclusive charged hadrons as a function of the transverse momentum p_T in comparison to PHOBOS [5] and PHENIX [6] data. Note the different centrality ranges of the data sets. All shown errors are statistical.

of produced hadrons creates zero elliptic flow, because the azimuthal distributions of secondaries in elementary hadron-hadron collisions are isotropic. The anisotropic flow, i.e., the azimuthal anisotropies of the number of produced hadrons, results from the spatial asymmetry of the collision zone and subsequent rescattering processes, which are crucial to converting the initial spatial anisotropy into the final momentum anisotropy. Hadronic rescattering including hard and multichain contributions creates an elliptic flow, which rises almost linearly according to the experimental data within the interval $0.0 \leqslant p_T \leqslant 1.0\,\mathrm{GeV}/c$, but saturates already for transverse momenta above $1.0\,\mathrm{GeV}/c$ at a level of $v_2^{\mathrm{ch}} \approx 6\%$, whereas the experimentally measured flow increases farther up to $v_2^{\mathrm{ch}} \approx 14$–$16\%$ where it declines for $p_T \geqslant 3.0\,\mathrm{GeV}/c$.

Although the model seems to describe the p_T dependence qualitatively well, it underestimates the experimental elliptic flow of charged particles with transverse momenta above $1.0\,\mathrm{GeV}/c$ roughly by up to 50%. What is the reason for these deviations? Recall that hadrons in the QGSM gain the transverse momentum due to (i) transverse motion of the constituent quarks and (ii) transverse momentum of constituents acquired in the course of string fragmentation. The parameters of these two processes are fixed by comparison with the available hadronic data. Other sources of the transverse motion are (iii) the transverse Fermi motion of nucleons in the colliding nuclei and (iv) rescattering of produced particles in the hot and dense nuclear medium. It was already mentioned that the latter process is the most crucial for the development of elliptic flow in nuclear reactions. However, secondary hadrons with high transverse momenta experience on average fewer collisions than their low-momentum counterparts because of the large formation time (which originates from the uncertainty principle). As shown in [42], in the limit of vanishing formation time the elliptic flow increases drastically. But all parameters linked to the formation time of produced particles in the QGSM are also fixed by comparison with experimental data on hadronic interactions. Therefore, the presented elliptic flow can be considered as an upper limit obtained within the hadronic cascade scenario. It clearly indicates new physical effects not taken into account by the microscopic model. Jets are among the most likely candidates for these processes. Indeed, as was discussed in [58], the nonuniform dependence of the energy loss on the azimuthal angle results in azimuthal anisotropy of jet spectra in noncentral nuclear collisions. This leads to a significant increase of the elliptic flow of high-p_T particles. Another possible explanation is, e.g., a dramatic increase of all s-channel transition rates in the vicinity of the chiral phase transition [59], which causes a critical opacity and fast thermalization in the system.

Finally, the centrality dependence of the total, i.e., η and p_T integrated v_2 for charged hadrons is depicted in the middle and right panels of Fig 10. Since the centrality of collision events in the experimental measurements [6] is characterized by the mean number of participants N_{part} (seen in the middle panel), we show in addition to this signal the original impact parameter dependence of the elliptic flow (right panel). The relation between the number of participants N_{part} in the Au+Au reactions and the impact parameter b of the simulated collisions is shown in the left panel of Fig 10. The number of nucleons

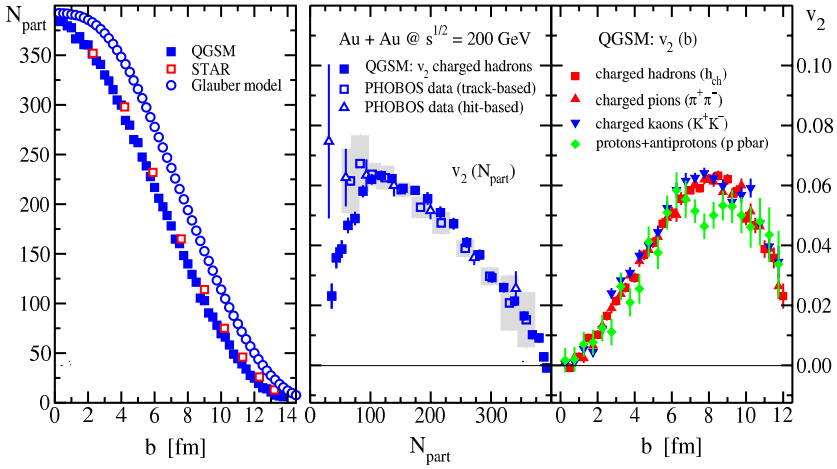

FIG. 10. (Color online) Centrality dependence of the elliptic flow v_2 for charged hadrons compared with the PHOBOS data [5] (middle panel), and v_2 of inclusive as well as identified charged hadrons as a function of the impact parameter b (right panel). The b dependence of the number of participants $N_{\rm part}$ is shown in the left panel (the STAR data are taken from [52]). The errors are statistical.

participating in inelastic scatterings, i.e., $N_{\rm part}$, is directly available in the QGSM. This number depends mainly on the nucleon-nucleon cross section, which for the given initial energy of $\sqrt{s_{NN}} = 200\,\text{GeV}$ is calculated in the framework of GRT. Apart from the cross section and its energy dependence, the number of participants varies with the impact parameter such as $\propto \exp(-b^2)$. Thus, the b dependence of $N_{\rm part}$ within the QGSM is rather different compared to the Glauber model result, but in nice agreement with the experimentally estimated $N_{\rm part}(b)$ [52]. Amazingly, the elliptic flow of inclusive charged hadrons extracted from our simulation almost coincides with the PHOBOS experimental data. This remarkable result in conjunction with the transverse momentum dependence of $v_2^{\rm ch}$ shown in Fig. 9 reflects the dominance of hadrons with low p_T. Furthermore, one can see that the elliptic flow as a function of the impact parameter b reaches a maximal value of around 6% at $b \approx 8$ fm, corresponding to $N_{\rm part} \approx 100$, and decreases with further increasing b. As expected, the flow in the midrapidity region is caused mainly by pions, but the azimuthal anisotropy parameters $v_2(b)$ for charged kaons and combined protons/antiprotons are also very similar within the statistical uncertainties. Note that the magnitude of the total pionic flow obtained within the QGSM simulations is more than twice as large as created by the RQMD ones [60].

IV. SUMMARY AND CONCLUSIONS

In summary, the pseudorapidity distributions of the azimuthal anisotropy parameters $v_1(\eta)$ and $v_2(\eta)$ of inclusive charged hadrons and their centrality dependence has been studied in Au+Au collisions at full RHIC energy of $\sqrt{s_{NN}} = 200\,\text{GeV}$ within the microscopic quark-gluon string model. The QGSM simulation results for the directed flow show antiflow alignment within the pseudorapidity range $|\eta| \leqslant 2$ in fair agreement with the experimental $v_1(\eta)$ data, but the QGSM cannot reproduce the further development of the antiflow up to $|\eta| \approx 3.5$. In a broad pseudorapidity region, the model generates a wiggle structure for the directed flow of nucleons v_1^N. At midrapidity $|\eta| \leqslant 1$, however, the generated flow is quite weak and consistent with the zero-flow behavior reported by the STAR and PHOBOS Collaborations. The η dependence of the elliptic flow v_2 extracted from our simulation agrees well with the experimental results in the whole η range for minimum bias as well as for central, midcentral, and peripheral collisions. The transverse momentum dependence of the elliptic flow $v_2(p_T)$ of identified $(\pi^{\pm}, K^{\pm}, p, \bar{p})$ and inclusive charged hadrons has also been investigated within the QGSM. The description by the quark-gluon string model is fairly good in the low-p_T range. Here, it was shown that for identified and charged hadrons, the v_2 parameter rises with increasing p_T according to the experimental data. For higher transverse momenta $p_T > 1\,\text{GeV}/c$, it starts rapidly to saturate already on a level, which is at the largest transverse momenta roughly 50% smaller than the experimentally measured v_2. On the other hand, the qualitative behavior of the elliptic flow in Au+Au collisions in the overall p_T range is well reproduced by the model. In particular, a striking feature of the QGSM is that it is able to describe qualitatively the different p_T dependence of the mesonic and baryonic elliptic flow and reproduces a crossing of the elliptic flow for mesons and baryons at $p_T > 1.4\,\text{GeV}$ observed in the PHENIX experiment at RHIC. The centrality dependence of the integrated elliptic flow of charged hadrons in the QGSM agrees almost perfectly with the PHOBOS experimental data. This fact reflects the dominance of low-p_T hadrons.

In conclusion, the microscopic quark-gluon string cascade model based on the color exchange mechanism for string formation is able to describe qualitatively and quantitatively well the bulk properties of the directed and elliptic flow measured in $\sqrt{s_{NN}} = 200\,\text{GeV}$ Au+Au collisions at RHIC. The limitations of the model should not permit a perfect agreement for all observables. The only signal that is really underestimated by the QGSM is the elliptic flow of hadrons with high transverse momenta $p_T > 1\,\text{GeV}/c$, although the v_2 of hadrons obtained within this model is already stronger than that of string models based on the FRITIOF scenario of excitation of longitudinal strings. The most plausible explanation of this discrepancy is an anisotropic character of jet absorption in a hot and dense asymmetric partonic medium. This effect, colloquially known as *jet quenching*, is being intensively studied now [1]. Other processes related

to the quark-hadron phase transition can be considered as well. The collective flow of hadrons appears to have a complex multicomponent structure caused by rescattering and absorption processes in a spatially anisotropic medium. Therefore, further detailed investigations of the freeze-out scenario for hadrons are required to understand properly the flow formation and its evolution.

ACKNOWLEDGMENTS

The authors are grateful to J. Aichelin, C. Greiner, L. Csernai, R. Lacey, and H. Stöcker for fruitful discussions and comments. This work was supported by the Bundesministerium für Bildung und Forschung (BMBF) under Contract 06TÜ986 and by the Norwegian Research Council (NFR).

[1] *Proceedings of the 17th International Conference on Ultra Relativistic Nucleus-Nucleus Collisions* (*Quark Matter 2004*), J. Phys. G **30**, S1 (2004).
[2] E. V. Shuryak, hep-ph/0011208; R. Stock, Nucl. Phys. **A661**, 282c (1999); U. Heinz, *ibid.* **A685**, 414 (2001).
[3] K. H. Ackermann *et al.* (STAR Collaboration), Phys. Rev. Lett. **86**, 402 (2001).
[4] I. Park *et al.* (PHOBOS Collaboration), Nucl. Phys. **A698**, 564c (2002); S. Manly *et al.*, *ibid.* **A715**, 614c (2003).
[5] B. B. Back *et al.* (PHOBOS Collaboration), nucl-ex/0407012.
[6] S. S. Adler *et al.* (PHENIX Collaboration), Phys. Rev. Lett. **91**, 182301 (2003).
[7] F. Karsch, Lect. Notes Phys. **583**, 209 (2002).
[8] E. Shuryak, Prog. Part. Nucl. Phys. **53**, 273 (2004).
[9] S. A. Voloshin, Nucl. Phys. **A715**, 379 (2003).
[10] P. F. Kolb, P. Huovinen, U. W. Heinz, and H. Heiselberg, Phys. Lett. **B500**, 232 (2001).
[11] P. Huovinen, P. F. Kolb, U. W. Heinz, P. V. Ruuskanen, and S. A. Voloshin, Phys. Lett. **B503**, 58 (2001).
[12] F. Retiere, J. Phys. G **30**, S827 (2004); T. Hirano, *ibid.* **30**, S845.
[13] B. Andersen, G. Gustafson, and B. Nielsson-Almqvist, Nucl. Phys. **B281**, 289 (1987).
[14] A. Capella, U. Sukhatme, C. I. Tan, and J. Tran Thanh Van, Phys. Rep. **236**, 225 (1994).
[15] V. Gribov, Sov. Phys. JETP **26**, 414 (1968); L. V. Gribov, E. M. Levin, and M. G. Ryskin, Phys. Rep. **100**, 1 (1983).
[16] L. V. Bravina, A. Faessler, C. Fuchs, and E. E. Zabrodin, Phys. Rev. C **61**, 064902 (2000); Phys. Lett. **B470**, 27 (1999).
[17] E. E. Zabrodin, C. Fuchs, L. V. Bravina, and A. Faessler, Phys. Rev. C **63**, 034902 (2001).
[18] H. Liu, S. Panitkin, and N. Xu, Phys. Rev. C **59**, 348 (1999).
[19] S. Soff, S. A. Bass, M. Bleicher, H. Stöcker, and W. Greiner, nucl-th/9903061.
[20] E. E. Zabrodin, C. Fuchs, L. V. Bravina, and A. Faessler, Phys. Lett. **B508**, 184 (2001).
[21] V. A. Abramovskii, V. N. Gribov, and O. V. Kancheli, Sov. J. Nucl. Phys. **18**, 308 (1974).
[22] N. S. Amelin, E. F. Staubo, and L. P. Csernai, Phys. Rev. D **46**, 4873 (1992).
[23] A. B. Kaidalov, Phys. Lett. **B116**, 459 (1982); A. B. Kaidalov and K. A. Ter-Martirosian, *ibid.* **B117**, 247 (1982); A. B. Kaidalov, Surv. in High Energy Phys. **13**, 265 (1999).
[24] N. S. Amelin, L. V. Bravina, L. I. Sarycheva and L. N. Smirnova, Sov. J. Nucl. Phys. **50** 1050 (1989); N. S. Amelin and L. V. Bravina, *ibid.* **51**, 133 (1990); N. S. Amelin, L. V. Bravina, L. P. Csernai, V. D. Toneev, K. K. Gudima, and S. Y. Sivoklokov, Phys. Rev. C **47**, 2299 (1993).
[25] C. M. Hung and E. V. Shuryak, Phys. Rev. Lett. **75**, 4003 (1995).
[26] D. H. Rischke and M. Gyulassy, Nucl. Phys. **A597**, 701 (1996).
[27] L. V. Bravina, N. S. Amelin, L. P. Csernai, P. Levai, and D. Strottman, Nucl. Phys. **A566**, 461c (1994).
[28] L. P. Csernai and D. Röhrich, Phys. Lett. **B458**, 454 (1999).
[29] N. S. Amelin, E. F. Staubo, L. P. Csernai, V. D. Toneev, K. K. Gudima, and D. Strottman, Phys. Rev. Lett. **67**, 1523 (1991).
[30] H. Sorge, Phys. Rev. Lett. **78**, 2309 (1997); **82**, 2048 (1999).
[31] L. V. Bravina, Phys. Lett. **B344**, 49 (1995).
[32] S. A. Voloshin and Y. Zhang, Z. Phys. C **70**, 665 (1996); S. A. Voloshin, Phys. Rev. C **55**, R1630 (1997).
[33] A. M. Poskanzer and S. A. Voloshin, Phys. Rev. C **58**, 1671 (1998).
[34] J.-Y. Ollitrault, Phys. Rev. D **46**, 229 (1992); **48**, 1132 (1993); Nucl. Phys. **A638**, 195c (1998).
[35] J. Adams *et al.* (STAR Collaboration), Phys. Rev. Lett. **92**, 062301 (2004).
[36] M. Belt Tonjes *et al.* (PHOBOS Collaboration), J. Phys. G **30**, S1243 (2004).
[37] L. V. Bravina, L. P. Csernai, A. Faessler, C. Fuchs, and E. E. Zabrodin, J. Phys. G **28**, 1977 (2002); Phys. Lett. **B543**, 217 (2002); L. V. Bravina, L. P. Csernai, A. Faessler, C. Fuchs, S. Panitkin, N. Xu, and E. E. Zabrodin, Nucl. Phys. **A715**, 665c (2003).
[38] R. J. M. Snellings, H. Sorge, S. A. Voloshin, F. Q. Wang, and N. Xu, Phys. Rev. Lett. **84**, 2803 (2000).
[39] E. Zabrodin, L. Bravina, C. Fuchs, and A. Faessler, Prog. Part. Nucl. Phys. **53**, 183 (2004).
[40] A. Wetzler *et al.* (NA49 Collaboration), Nucl. Phys. **A715**, 583 (2003).
[41] C. Alt *et al.* (NA49 Collaboration), Phys. Rev. C **68**, 034903 (2003).
[42] M. Bleicher and H. Stöcker, Phys. Lett. **B526**, 309 (2002).
[43] L. W. Chen, V. Greco, C. M. Ko, and P. F. Kolb, Phys. Lett. **B605**, 95 (2005).
[44] V. K. Magas, L. P. Csernai, and D. Strottman, Nucl. Phys. **A712**, 167 (2002).
[45] B. B. Back *et al.* (PHOBOS Collaboration), Phys. Rev. Lett. **91**, 052303 (2003).
[46] B. B. Back *et al.* (PHOBOS Collaboration), nucl-ex/0410022.
[47] P. Huovinen, review for *Quark-Gluon Plasma 3*, edited by R. C. Hwa and X. -N. Wang (World Scientific, Singapore, 2004), nucl-th/0305064.
[48] T. Hirano and K. Tsuda, Nucl. Phys. **A715**, 821 (2003).
[49] T. Hirano and K. Tsuda, Phys. Rev. C **66**, 054905 (2002).
[50] T. Hirano, Phys. Rev. C **65**, 011901(R) (2001).
[51] L. Bravina, K. Tywoniuk, E. Zabrodin, G. Burau, J. Bleibel, C. Fuchs, and A. Faessler, hep-ph/0412343.
[52] J. Adams *et al.* (STAR Collaboration), nucl-ex/0409033.

[53] J. Adams *et al*. (STAR Collaboration), Phys. Rev. Lett. **92**, 112301 (2004).
[54] D. Molnar and M. Gyulassy, Phys. Rev. C **62**, 054907 (2002); D. Molnar and S. A. Voloshin, Phys. Rev. Lett. **91**, 092301 (2003).
[55] V. Greco, C. M. Ko, and P. Levai, Phys. Rev. C **68**, 034904 (2003).
[56] R. J. Fries, B. Müller, C. Nonaka, and S. A. Bass, Phys. Rev. C **68**, 044902 (2003).
[57] R. C. Hwa and C. B. Yang, Phys. Rev. C **67**, 034902 (2003).
[58] I. P. Lokhtin, S. V. Petrushanko, L. I. Sarycheva, and A. M. Snigirev, Pramana **60**, 1045 (2002); I. P. Lokhtin, L. I. Sarycheva, and A. M. Snigirev, Phys. Lett. **B537**, 261 (2002).
[59] F. Gastineau, E. Blanquier, and J. Aichelin, hep-ph/0404207.
[60] R. J. M. Snellings, A. M. Poskanzer, and S. A. Voloshin, nucl-ex/9904003.